Chemical Engineering Journal 545 (2026) 179422

Contents lists available at ScienceDirect

Chemical Engineering Journal

journal homepage: www.elsevier.com/locate/cej

Epitaxial high-entropy relaxor ferroelectric films for flexible piezoelectric sensors and MEMS

Yu-En Pan [a], Yu-Hao Tu [a], Li-Hui Tsao [b], Yu-Ju Lin [c], Sheng-Yao Hung [d], Yi-Chun Chen [e,d], Mengyao Xiao [f,g,h], Qibin Zeng [h], Huajun Liu [h,i], Chengkuo Lee [f,g], Ying-Hao Chu [a,b,*]

[a] College of Semiconductor Research, National Tsing Hua University, No.101, Section 2, Kuang-Fu Road, Hsinchu, 300044, Taiwan
[b] Department of Materials Science and Engineering, National Tsing Hua University, No.101, Section 2, Kuang-Fu Road, Hsinchu, 300044, Taiwan
[c] Department of Materials Science and Engineering, National Yang Ming Chiao Tung University, No.101, Section 2, Kuang-Fu Road, Hsinchu, 300044, Taiwan
[d] Department of Physics, National Cheng Kung University, Tainan, 70101, Taiwan
[e] Center for Quantum Frontiers of Research and Technology (QFort), Tainan, 70101, Taiwan
[f] Department of Electrical and Computer Engineering, National University of Singapore, Singapore, 117576, Singapore
[g] Centre for Intelligent Sensors and MEMS (CISM), National University of Singapore, Singapore, 117583, Singapore
[h] Institute of Materials Research and Engineering (IMRE), Agency for Science, Technology and Research (A*STAR), 2 Fusionopolis Way, Innovis #08-03, Singapore, 138634, Singapore
[i] School of Materials Science and Engineering, 50 Nanyang Avenue, Nanyang Technological University, Singapore, 639798, Singapore

ARTICLE INFO

Keywords:
High-entropy
Relaxor ferroelectric
Piezoelectric
Flexible sensors

ABSTRACT

Flexible high-entropy relaxor ferroelectrics offer a promising route to overcome the long-standing challenges between mechanical flexibility, thermal stability, and electromechanical performance in piezoelectric applications. In this study, we demonstrate the novel van der Waals (vdW) epitaxial integration of a designed high-entropy oxide, $Pb(Mg_{0.15}Nb_{0.3}Ti_{0.05}Hf_{0.25}Zr_{0.25})O_3$ (PMNTHZO), onto flexible muscovite (mica) and rigid silicon substrates. Through high-entropy engineering, these films exhibit excellent epitaxial crystallinity and a significantly enhanced breakdown electric field ($>$ 4 MV cm^{-1} on silicon). By exploiting the vdW interfacial sliding on mica to decouple substrate clamping, the PMNTHZO films achieve an exceptionally large effective piezoelectric coefficient ($d_{33,\ eff} \approx 118 \pm 6$ pm V^{-1}). PMNTHZO maintains stable polarization switching above 250 °C and exhibits remarkable mechanical durability, surviving a bending radius of 3.5 mm for over 10,000 continuous deformation cycles. Validated by thickness-dependent analyses and fabricated micro-island structures that explicitly confirm the mitigation of the substrate clamping effect on mica, these results establish PMNTHZO as a robust, thermally stable, and highly flexible piezoelectric material, paving the way for next-generation harsh-environment MEMS and wearable sensors.

1. Introduction

Piezoelectric sensors and microelectromechanical systems (MEMS) have been indispensable in modern technologies ranging from consumer electronics to biomedical monitoring and human-machine interfaces. With growing demands for miniaturized, high-sensitivity, and multifunctional devices, high-performance piezoelectric materials are now a key component of next-generation MEMS [1]. Recently, advances in flexible and wearable devices have intensified research into materials that combine strong electromechanical coupling, mechanical flexibility, and reliable operation under diverse thermal and environmental conditions. Conventional piezoelectric materials such as $Pb(Zr_{1-x}Ti_x)O_3$ (PZT) films offer relatively high piezoelectric responses ($d_{33} \approx$ 30–50 pm V^{-1}) [2,3]. However, their intrinsically rigid and brittle nature constrains their utility in wearable and deformable systems. Similarly, as another representative ceramic piezoelectric material, $BaTiO_3$, typically exhibits practical d_{33} values of 10–70 pm V^{-1}, which are strongly influenced by factors such as film thickness, substrate clamping, and electrode configuration [4–6], yet their performance remains fundamentally limited by the mechanical inflexibility of oxides. In contrast,

* Corresponding author at: College of Semiconductor Research, National Tsing Hua University, No.101, Section 2, Kuang-Fu Road, Hsinchu, 300044, Taiwan.
E-mail addresses: yepan@gapp.nthu.edu.tw (Y.-E. Pan), dennistu1223@gapp.nthu.edu.tw (Y.-H. Tu), nthu031239@gmail.com (L.-H. Tsao), carol.ju88.en13@nycu.edu.tw (Y.-J. Lin), L28141529@gs.ncku.edu.tw (S.-Y. Hung), ycchen93@mail.ncku.edu.tw (Y.-C. Chen), e1143591@u.nus.edu (M. Xiao), qibin_zeng@a-star.edu.sg (Q. Zeng), liu_huajun@a-star.edu.sg (H. Liu), elelc@nus.edu.sg (C. Lee), yhchu@mx.nthu.edu.tw (Y.-H. Chu).

https://doi.org/10.1016/j.cej.2026.179422
Received 23 February 2026; Received in revised form 10 May 2026; Accepted 11 July 2026
Available online 14 July 2026

flexible piezoelectric polymers (e.g., PVDF, PLA, and glycine-polycaprolactone) offer excellent mechanical compliance but suffer from modest piezoelectricity ($d_{33} < 40$ pm V^{-1}) and severe thermal degradation at relatively low temperatures (e.g., PVDF degrades above 70–80 °C) [7–11]. These limitations hinder their applicability in high-performance and harsh-environment sensor devices. As a result, current piezoelectric materials suffer from an inherent compromise among electromechanical performance, flexibility, and thermal stability. While rigid oxide ceramics are prone to fracture under mechanical strain, flexible polymers typically degrade at elevated temperatures and fail to meet demanding sensing requirements.

To resolve this, one might consider integrating traditional high-performance relaxors, such as $Pb(Mg_{1/3}Nb_{2/3})O_3$-$PbTiO_3$ (PMN-PT), onto flexible substrates. However, standard PMN-PT systems possess a relatively low Curie temperature ($T_C \approx 130$–150 °C) [12,13], severely restricting their operational window.

To bridge this gap and overcome the limitations of both flexible polymers and traditional PMN-PT, high-entropy systems have emerged as a uniquely suited solution that reconciles high piezoelectricity with environmental robustness. In this work, we introduce Hf and Zr ions into a PMN-PT-based system to create a high-entropy oxide, $Pb(Mg_{0.15}Nb_{0.3}Ti_{0.05}Hf_{0.25}Zr_{0.25})O_3$ (PMNTHZO). This concept exploits the increase in configurational entropy that arises from mixing multiple elements, thereby lowering the free energy and promoting the formation of stable solid-solution phases [14]. The multi-elements with different ionic sizes introduce severe lattice distortion and a nonperiodic atomic distribution. Crucially, for flexible and harsh-environment applications, this severe distortion not only increases the activation energy for ion migration, thereby suppressing defect-mediated leakage, but also inherently impedes crack propagation and stress concentrations under mechanical deformation. The sluggish diffusion effect arises from competition among multiple atomic species, and lattice distortion hinders atomic diffusion, slowing phase transitions and the growth of oxygen vacancies, further stabilizing the perovskite structure against high-temperature degradation [14–16]. However, realizing such oxide films typically requires high-temperature processing, which is incompatible with conventional polymer substrates. To overcome this bottleneck, we utilize muscovite mica as the substrate. Mica offers exceptional thermal stability ($T_m \approx 1000$ °C) [17] and mechanical flexibility at ultra-thin thicknesses [17,18], making it an ideal platform for realizing high-temperature-resilient, flexible high-entropy piezoelectric devices. Furthermore, compared to standard PMN-PT, PMNTHZO exhibits superior epitaxial quality and significantly reduced leakage currents when grown on mica. This makes PMNTHZO a far more comprehensive and preferred material for simultaneously addressing the challenges of thermal stability, mechanical flexibility, and high piezoelectric performance.

Recent studies have explored high-entropy oxides and perovskites as active layers in resistive switching [19], dielectric capacitors [20], and multifunctional coatings and thin films [21]. However, the integration of high-entropy oxides with flexible substrates remains largely unexplored, and their operating temperatures are severely constrained by the softness of these substrates. For instance, Yang et al. reported that high-entropy $TiVCrMoC_3T_x$ MXene–PVA films deliver strong piezoresponse and mechanical compliance. Yet their polymer-bound crystallinity and limited thermal tolerance restrict device operating windows [22]. Pratihar et al. demonstrated $(Bi_{0.2}Na_{0.2}Ba_{0.2}K_{0.2}La_{0.2})TiO_3$/PVDF sensors similarly enhance dipole activity ($d_{33} \approx 33$ pm V^{-1}), though the soft polymer matrix imposes constraints on high-temperature stability [23]. Very limited studies have focused on integrating high-entropy oxides with flexible materials while simultaneously probing their electromechanical and thermal stability. To address this critical gap and bridge traditional rigid microsystems with emerging flexible electronics, we successfully grew the PMNTHZO high-entropy system on both silicon and flexible mica substrates. The integration on the Si substrate achieves an exceptionally high breakdown electric field and validates CMOS compatibility, demonstrating the strong potential and fundamental suitability of PMNTHZO for future integration into next-generation MEMS. Meanwhile, the mica substrate demonstrates remarkable resilience at high temperatures, serving as a tangible demonstration of flexible sensors. This confirms the robustness of high-entropy design across both rigid and flexible architectures.

PMNTHZO is a prospective high-entropy relaxor ferroelectric material with superior thermal stability and epitaxial quality [24]. To further broaden the application landscape of this material, we epitaxially grew PMNTHZO on flexible mica and silicon substrates (Fig. 1c and d). Silicon was selected to validate CMOS compatibility with established MEMS technologies [25–27], while mica enables van der Waals epitaxy of high-quality oxides, ensuring mechanical compliance without sacrificing thermal limits [28,29]. In this work, the epitaxial thin films were characterized by X-ray diffraction (XRD) and transmission electron microscopy (TEM). The ferroelectric and piezoelectric behaviors of PMNTHZO were characterized with thermal and bending tests. PMNTHZO exhibits a significantly enhanced piezoresponse ($d_{33,\ eff} \approx 118 \pm 6$ pm V^{-1}) and maintains over 80% performance of its ferroelectric polarization at 250 °C. Our results reveal that a high-entropy relaxor design can overcome the challenges of integrating flexibility, crystallinity, and functional performance, as the concept presented in Fig. 1a. We developed a new pathway toward multifunctional and thermally stable piezoelectric devices, thereby expanding the potential of high-entropy materials.

This table summarizes typical piezoelectric materials reported for MEMS and wearable applications [2–9,30–41]. Materials such as PZT and $BaTiO_3$ exhibit decent piezoelectric performance but are inherently rigid, which limits their use in flexible devices. Polymer-based piezoelectrics, including PVDF, PLLA, and PHB, are mechanically compliant and biocompatible, but their weak electromechanical coupling restricts sensing performance. Acoustic MEMS materials such as AlN and $LiNbO_3$ are well established in RF and ultrasonic devices, yet they lack flexibility. In this work, PMNTHZO stands out by simultaneously offering high piezoelectricity, flexibility and CMOS compatibility, enabling new opportunities for both MEMS and wearable sensors.

2. Material and methods

2.1. Thin-film growth

Epitaxial PMNTHZO, $SrRuO_3$ (SRO), and $SrTiO_3$ (STO) thin films were deposited on silicon and mica using a pulsed laser deposition system equipped with a KrF excimer laser ($\lambda = 248$ nm). During the deposition process, the specific laser energy density was maintained at ~2 J cm^{-2}, with a repetition rate of 10 Hz and a target-to-substrate distance of 4.5 cm. The PMNTHZO films were grown at an oxygen partial pressure of 100 mTorr and a substrate temperature of 600 °C, yielding film thicknesses of ~180 nm on Si (100) and ~ 300 nm on mica substrates. A 60 nm SRO bottom electrode layer was deposited at 680 °C under the same oxygen pressure. For mica-based samples, a 60 nm STO seed layer was first grown at 650 °C to facilitate van der Waals epitaxy and improve the crystallinity of the subsequent functional layers. After deposition, all samples were cooled to room temperature in oxygen (100 mTorr) to promote full oxidation of the films.

2.2. Structural characterization

Room-temperature XRD measurements were performed to evaluate the crystallinity and epitaxial orientation of the thin films. θ–2θ scans were performed using a Bruker D2 diffractometer to identify out-of-plane orientations by measuring constructive interference under Bragg's law. ϕ-scans were carried out using a Rigaku diffractometer to probe the in-plane symmetry and epitaxial relationship between the films and substrates. Cross-sectional microstructural analyses were performed using TEM (JEOL JEM-F200). Samples were prepared via FIB

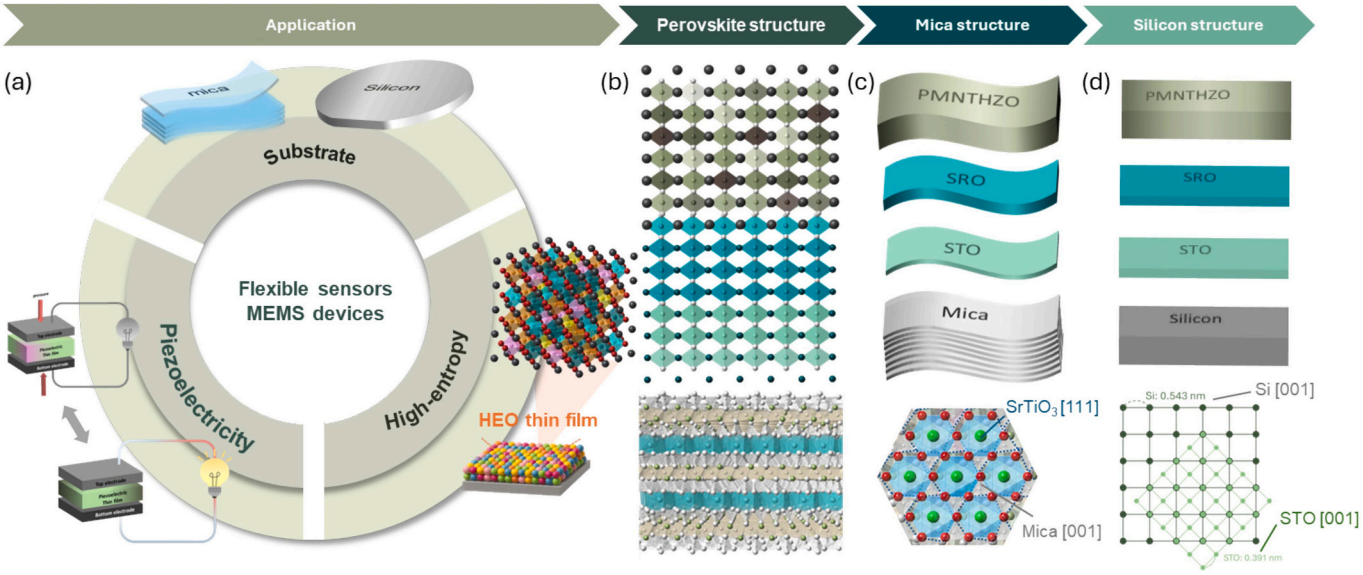

Fig. 1. (a) Applications for sensors and MEMS. (b) Perovskite structures of STO, SRO, PMNTHZO (c) Mica-based structure (d) Silicon-based structure and crystal stacking profiles.

(Zeiss Crossbeam 550) milling, and TEM imaging was used to capture the heterostructure of thin-film interfaces and to obtain diffraction patterns via FFT, which provides a clear explanation of the epitaxial relationship between each film. Elemental distribution and high-entropy compositional uniformity were confirmed using EDS/TEM, as presented in the Supporting Information.

2.3. Ferroelectric measurements

P-E hysteresis loops were acquired using a TF Analyzer 3000 (aixACCT Systems). Measurements were performed under voltages from −72 V to +72 V. To account for substrate- dependent dielectric properties, AC excitation frequencies of 15 kHz for Si-based films and 10 kHz for mica-based films were employed. These measurement parameters allowed clear identification of relaxor ferroelectric behavior, including slim hysteresis loops and stable high-field switching.

2.4. Piezoelectric characterization

Macroscopic piezoelectric output currents were measured by a source meter (Keithley 2400) during controlled bending and tactile experiments to evaluate the strain-to-current signal. The piezoresponse under cyclic bending and hand deformation was recorded to assess mechanical robustness and fatigue stability. Nanoscale piezoelectric properties were further characterized by piezoresponse force microscopy (PFM) (cypher AFM), enabling direct extraction of the effective out-of-plane piezoelectric coefficient ($d_{33,\ eff}$) under switching spectroscopy in the dual AC resonance tracking (DART) PFM mode. Meanwhile, the effective $d_{33,\ eff}$ vs DC bias loop curve was measured by a LDV system (OFV-5000, Polytec), where a sinusoidal AC drive (1 kHz, 1 V_{pp}) superimposed with a varying DC bias was applied. For these electrical and electromechanical evaluations, top electrodes were fabricated by sputtering Au (20 nm)/Pd (15 nm) and patterned via a shadow mask to achieve a 200 μm diameter. To ensure the high repeatability and reproducibility of our results, all quantitative electromechanical and electrical measurements were conducted on at least three different devices across three independently fabricated sample batches. In all corresponding figures, the error bars represent the standard deviation.

3. Results

3.1. Structural characterization

Two distinct sets of heteroepitaxies were fabricated to investigate the properties of PMNTHZO thin films. The first architecture consists of PMNTHZO/SRO/STO/mica (Fig. 1c), representing a flexible device configuration. In contrast, the second set was grown on a rigid silicon substrate with the same multilayer stack (Fig. 1d). In both systems, a STO layer was introduced as the seed layer to facilitate high-quality epitaxial growth by mitigating lattice mismatch. Subsequently, a conductive SRO layer was deposited as the bottom electrode before the growth of the functional PMNTHZO film. Fig. 2a presents the θ–2θ diffraction profiles. The film grown on Si (001) displays distinct (00L) reflections, indicating a highly oriented out-of-plane texture guided by the crystalline Si surface. The absence of a secondary orientation signal confirms that the film adopts a single preferred texture, consistent with conventional epitaxial growth with strong interfacial bonding. In contrast, the film deposited on mica exhibits a single set of (111) and (222) reflections, demonstrating a pure (111) out-of-plane texture. According to the previous PMNTHZO study, PMNTHZO is expected to have a pseudocubic structure [24]. To quantitatively evaluate the strain effect within the epitaxial films, reciprocal space mapping (RSM) was conducted to extract the in-plane (a_{ip}) and out-of-plane (a_{oop}) lattice parameters (Fig. S1 and Table S1). Because PMNTHZO is a novel high-entropy oxide system, a standardized bulk lattice parameter (a_0) is not yet available in crystallographic databases to calculate absolute strain percentages. Therefore, dimensional relaxation was analyzed. The extracted lattice parameters are $a_{ip} \approx 0.414$ nm and $a_{oop} \approx 0.410$ nm on a rigid STO substrate, and $a_{ip} \approx 0.416$ nm and $a_{oop} \approx 0.411$ nm on the flexible mica substrate. No significant difference in lattice distortion was observed. The films are all relaxed due to a large lattice mismatch with STO (0.39 nm) and the van der Waals nature of mica. To examine in-plane crystallographic alignment, ϕ-scans (Fig. 2c and f) were performed on asymmetric {110}-type reflections. The ϕ-scan of the {110} reflections shows that PMNTHZO and SRO share the same fourfold symmetry, while the Si peaks appear rotated by 45°. This rotation originates from the STO buffer layer adopting a 45° in-plane alignment [42], where the STO [100] axis matches the Si [110] direction to achieve a reduced lattice mismatch of 1.66% ($0.391 \times \sqrt{2} = 0.552$ nm vs. 0.543 nm for Si) [42,43]. As a result, the rotated epitaxial relationship at the

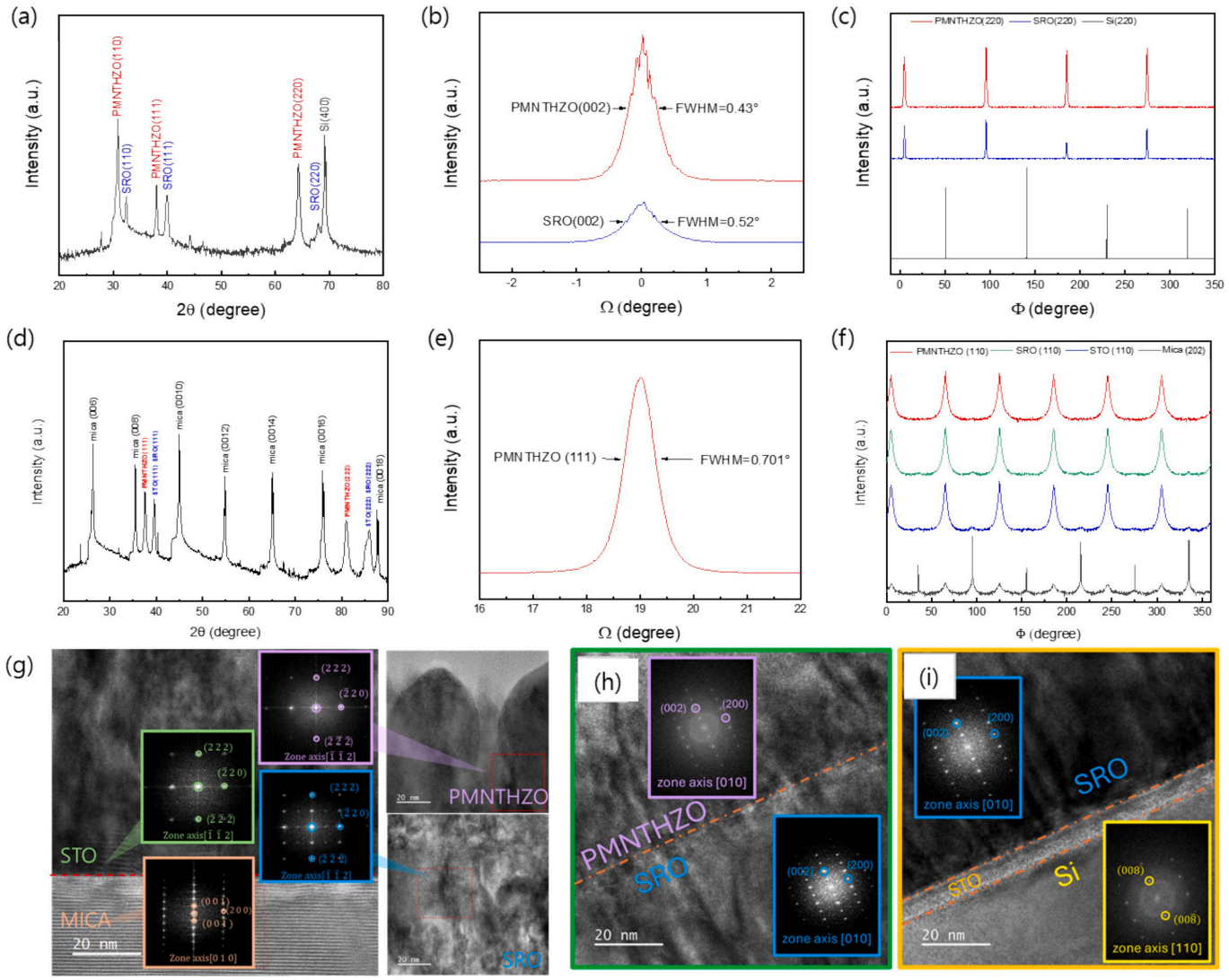

Fig. 2. Structural characteristic of PMNTHZO. (a) Out-of- plane XRD θ-2θ scan heterostructure of PMNTHZO on silicon. (b) Rocking curves of PMNTHZO (002) and SRO (002). (c)Φ-scan of silicon (220), SRO (220), and PMNTHZO (220). (d) Out-of- plane XRDθ-2θ scan heterostructure of PMNTHZO on mica. (e) Rocking curves of PMNTHZO (111). (f) Φ-scan of mica (202), SRO (110), STO (110), and PMNTHZO (110). (g) Cross-sectional TEM images of PMNTHZO on mica with corresponding FFT patterns. (h) (i) Cross-sectional TEM images of PMNTHZO on silicon with corresponding FFT patterns.

STO/Si interface is transferred upward, dictating the in-plane orientation of the entire heterostructure. In contrast, the ϕ-scan from the film on mica shows sixfold rotational symmetry, characteristic of (111)-oriented perovskite films [44,45]. The crystalline quality was further evaluated via rocking-curve measurements (Fig. 2b and e). The Si-based film exhibits a narrow full width at half maximum (FWHM) of 0.43°, indicative of excellent crystallinity and a coherent epitaxial interface. The mica-based film shows a slightly broader FWHM of 0.7°. While wider than that of Si, this value is remarkably low given the substantial lattice mismatch (> 4%) between STO and mica [44,45]. This high-quality growth is attributed to van der Waals epitaxy (vdWE). Unlike conventional epitaxy, which relies on rigid interfacial chemical bonding [46], vdWE utilizes weak vdW interactions that tolerate significant lattice mismatches [28]. Consequently, even with considerable lattice mismatch, the PMNTHZO film on mica retains high structural integrity and relaxes interface-induced strain, both of which are critical for flexible applications.

The epitaxial relationship and microstructure of silicon and mica-based films were verified through TEM. Fig. 2g, h and i show the cross-sectional TEM images and corresponding diffraction patterns, taken in the direction of [110] $_{\text{Silicon}}$ and [010] $_{\text{mica}}$. The corresponding FFT patterns exhibit well-defined diffraction spots without noticeable secondary phases, confirming an excellent epitaxial relationship between each film. High-entropy composition in the PMNTHZO film was confirmed by energy-dispersive X-ray spectroscopy (EDS) (Fig. S2) [24], which reveals a spatially uniform distribution of all atomic species. This high-entropy configuration plays a vital role in the material's relaxor ferroelectric behavior. The random distribution of multiple cations (Mg, Nb, Ti, Hf, Zr) at the B-site induces severe lattice distortion and generates local random electric fields. These random fields suppress the formation of long-range ferroelectric order, instead promoting the formation of polar nano-regions (PNRs), which is a signature of relaxor ferroelectrics [24,47–49]. PFM provides direct visualization of this phenomenon (Fig. S3). Unlike the macro-domains typical of classical ferroelectrics, the PMNTHZO films display a nanoscale domain structure (few nanometers) [49]. These highly dynamic PNRs facilitate easy polarization rotation under external fields. Specifically, the high-entropy incorporation of multiple elements lowers local crystal symmetry and reduces the material's structural anisotropy, allowing previously constrained polarization vectors to become far more flexible and easier to rotate [47,48]. This is the fundamental mechanism responsible for the enhanced piezoelectric response [50] and high thermal stability

discussed in the following sections (Table 1).

3.2. Enhanced breakdown electrical field and thermal stability

The measured polarization-electric field (P-E) hysteresis loops exhibit a characteristic slim and pinched shape, distinct from the square-like loops typically observed in conventional ferroelectrics. As shown in Fig. 3, the PMNTHZO films under an electric field of 0.8 MV cm^{-1} exhibit small remanent polarization ($P_r \approx 0.5$ μC cm^{-2}) and coercive field ($E_c \approx 0.11$ MV cm^{-1}), while maintaining a high saturated polarization ($P_s \approx 35$ μC cm^{-2}). This hysteresis behavior is a hallmark of relaxor ferroelectrics, indicating the absence of stable long-range ferroelectric order at zero bias. Besides, owing to the high-entropy design, PMNTHZO relaxor films exhibit simultaneously enhanced breakdown strength (E_b), enabling reliable operation under high electric fields ($E_b \approx 4$ MV cm^{-1} on silicon and 2.21 MV cm^{-1} on mica, Fig. 3a and b). In bulk high-entropy relaxor ceramics, multi-cation incorporation with diverse ionic radii and valences has been shown to disrupt long-range ferroelectric macrodomains [51], generate dense polar nano-regions, and refine grains, thereby increasing grain and grain-boundary activation energies, boosting breakdown strength, and reducing leakage [51,52]. The epitaxial film provides a dense structure with minimal defects, thereby intrinsically reducing leakage conduction [53]. With high-entropy design, the severe lattice distortion induced by the size and charge mismatch of the five B-site cations [15] acts as an effective scattering centers for charge carriers, which also intrinsically suppresses leakage conduction paths [52,54]. By leveraging these mechanisms, the high-entropy PMNTHZO films behave as superior relaxors, offering larger polarization, a slimmer hysteresis loop, and a higher breakdown electric field, all of which are favorable for achieving stronger piezoelectric responses in devices at high fields.

To clarify the physical origin of the enhanced breakdown strength, quantitative leakage current analyses were conducted, comparing the PMNTHZO film with a conventional epitaxial PZT control sample (detailed J-V characteristics and Poole-Frenkel emission fitting plots are shown in Figs. S4 and S5). The analysis reveals that the leakage mechanism at high electric fields and temperatures is dominated by Poole-Frenkel emission. The extracted thermal activation energy for PMNTHZO is exceptionally high (≈ 0.98 eV), indicative of deep trap levels originating from the high-entropy configuration [55,56]. In stark contrast, the epitaxial PZT film exhibits significantly lower activation energy (≈ 0.26 eV), corresponding to shallow trap levels [57,58]. Because both films share high epitaxial quality, this substantial difference provides direct evidence that the severe lattice distortion and sluggish diffusion inherent in the high-entropy design intrinsically alter the band structure. These robust deep traps effectively confine charge carriers, requiring significantly higher energy to trigger breakdown, which provides a physical explanation for the superior electrical and thermal stability of PMNTHZO up to 250 °C.

According to the previous study, similar relaxor ferroelectric systems exhibited promising thermal robustness [24], thereby motivating a detailed investigation into how high-entropy engineering enhances structural and functional stability at high temperatures. Both the silicon and mica-based films retain relaxor ferroelectric switching behavior at 250 °C (Fig. 3c and d), as evidenced by the well-defined P-E loops, demonstrating their robust high-temperature stability. First, this behavior is consistent with the intrinsic characteristics of relaxor ferroelectrics, in which the phase transition occurs via a diffuse, compositionally driven process rather than the abrupt structural change typical of classical ferroelectrics [59,60]. Unlike traditional ferroelectrics that undergo sudden macroscopic depolarization at their Curie temperature, this highly diffuse transition effectively suppresses abrupt depolarization [61]. This allows the material to retain its functional polarization over a much broader temperature window, making relaxor systems intrinsically more suitable for high-temperature piezoelectric operation [51,59,60,62]. Second, the high configurational entropy leads to sluggish diffusion and severe local lattice distortion, enhancing the thermal resistance of PMNTHZO [14–16,19]. The sustained remanent polarization and coercive field observed at elevated temperatures (Fig. 3c) are strongly consistent with the thermodynamic stabilization mechanisms characteristic of high-entropy engineering. Therefore, this high thermal limit is strongly attributed to the high-entropy relaxor design, ensuring reliable performance in harsh environment applications.

3.3. Ferroelectrics on flexible mica

To evaluate the mechanical robustness of the PMNTHZO film on mica, we conducted a series of bending-dependent electrical measurements, including polarization switching under different bending radii, and retention and fatigue cycling at a fixed bending radius of 5 mm. The P-E loops obtained under bending radii down to 15–3.5 mm (Fig. 3e and f) show negligible changes in saturated (1.72% variation), remnant polarization (0.61% variation), and coercive field (0.81% variation). This indicates that the epitaxial film maintains stable ferroelectric switching even under mechanical strain. To fully appreciate this flexibility, the position of the mechanical neutral plane should be taken into account. In this heterostructure, the total thickness of the functional epitaxial layers (PMNTHZO/SRO/STO) is approximately 420 nm, which is negligible compared to the thickness of the mica substrate (≈ 30 ± 10 μm). Consequently, the mechanical neutral plane is located near the geometric center of the mica substrate, leaving the PMNTHZO film positioned at the outermost surface where it experiences the maximum tensile or compressive strain ($\epsilon_{3.5mm} \approx \pm(0.43 \pm 0.14)\%$) during bending. Despite being subjected to this maximum strain at a bending

Table 1
Comparison of representative piezoelectric materials for MEMS and wearable applications.

Materials	d_{33}	CMOS Compatibility	Flexibility	Device Type	MEMS Application	Wearable Application	Ref.
PZT	30–50 pm V^{-1}	No	No	MEMS	Actuators, pressure sensors, accelerometers, PMUTs, energy harvesters	Wearable pressure sensing, motion monitoring, voice recognition (transfer/bonding only)	[2,3,30,31]
$BaTiO_3$	10–70 pm V^{-1}	Yes	No	MEMS	Pressure sensors, micro-actuators, energy harvesters	Flexible composites with polymer matrices (strain/pressure sensing)	[32–34]
PVDF	24 to 34 pC N^{-1}	Yes	Yes	MEMS & Wearable	MEMS resonators, acoustic microsensors	Strain/pressure, pulse, motion, HMI, tactile sensing	[7,8,35–37]
PLLA	3.1 pC N^{-1}	Yes	Yes	Wearable	–	Biocompatible strain sensing, implantable sensors	[9,39]
AlN	3.9 pm V^{-1}	Yes	No	MEMS	FBAR/SMR RF filters, SAW devices, PMUTs, pressure sensors	–	[40,41]
$LiNbO_3$	16 pm V^{-1}	No	No	MEMS	MEMS resonators, SAW/BAW RF filters,	–	[40]
PMNTHZO	≈ 100 pm V^{-1}	Yes	Yes	MEMS & Wearable	–	–	This work

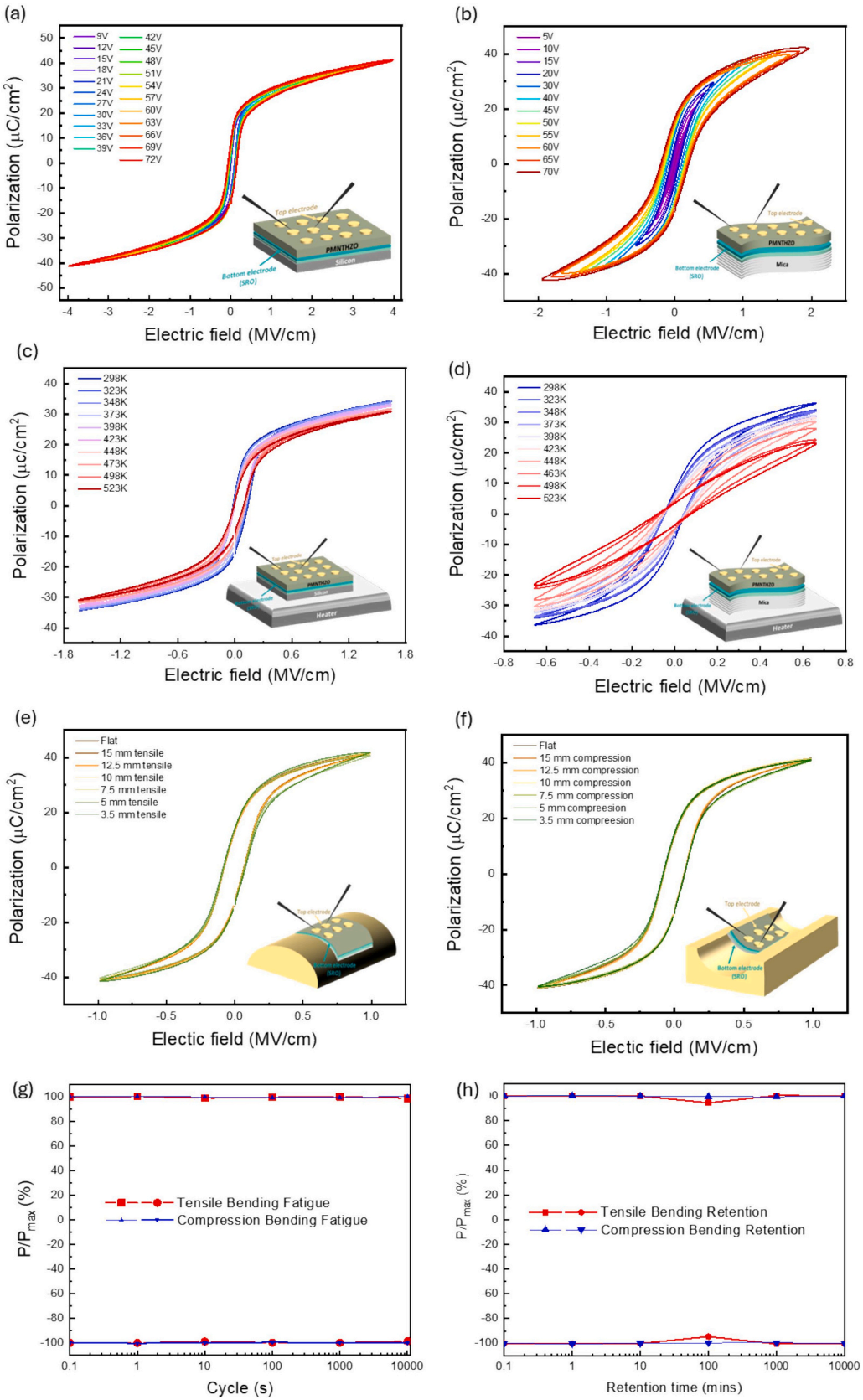

Fig. 3. Ferroelectric properties of PMNTHZO. The P-E results of PMNTHZO on (a) silicon and (b) mica at various electric fields. Varied temperature-PE results of PMNTHZO on (c) silicon and(d) mica. Flexibility test results of (e) tensile state and (f) compressive state P-E on mica. (g) Cycling fatigue test performed at the same radius over 10,000 bending cycles. (h) 10,000 min of continuous bending.

radius of 3.5 mm, the device maintains its structural integrity and functional performance. This remarkable invariance highlights the mechanical flexibility of the mica-based heterostructure. Mica was reported to bend at a radius of 0.3 mm with a thickness of 100 nm [17] or to remain stable at bending radii of 2.5 mm or 3.5 mm [29,63]. The weak vdW interfacial bonding and the atomically flat nature [28,29] of the substrate act as a mechanical buffer layer that permits slight interfacial sliding, mitigating the strain concentration and crack propagation mechanisms that frequently impair ferroelectric oxides grown on rigid substrates.

At a fixed bending radius of 5 mm, the device further demonstrates excellent retention stability. A cycling fatigue test (Fig. 3g) performed at the same radius shows that the film withstands over 10,000 bending cycles without changes in polarization. Fig. 3h shows nearly identical polarization values after 10,000 min of continuous bending. Such long-term reliability under repeated mechanical deformation is rarely observed in conventional perovskite ferroelectric systems grown on polymer substrates, where thermal mismatch, grain-boundary sliding, or interfacial delamination often limit electrical endurance. The superior stability observed here is attributed to mica's unique properties. It has high intrinsic flexibility and mechanical resilience, which preserves ferroelectric property even during cyclic deformation. Previous studies on oxide films grown on mica, such as epitaxial $BaTiO_3$ [64], $BiFeO_3$ (BFO) [65], or PZT [66] systems, have also shown that the pseudo-hexagonal layered structure enables uniform strain distribution and robust structures during cyclic deformation, consistent with our observations. These results confirm that the PMNTHZO/mica heterostructure can sustain prolonged dynamic stress while retaining its ferroelectric characteristics, highlighting the promise of mica-based van der Waals epitaxy for next-generation flexible ferroelectric and piezoelectric devices.

3.4. Piezoelectric PMNTHZO films

We utilized mica substrates with a thickness of 20–30 μm, which provides excellent flexibility for fabricating the piezoelectric device (Fig. 4a). To fully evaluate the piezoelectricity of PMNTHZO, the piezoelectric performance was comprehensively characterized through both macroscopic mechanical measurements and nanoscale analysis. First, the device maintained nearly identical output after 1000 repeated bending cycles (Fig. 4b), confirming the mechanical robustness and fatigue resistance of the PMNTHZO/mica heterostructure. Fig. 4c illustrates the output current response of the PMNTHZO film on mica subjected to the external bending stage. As the bending radius decreased from 17 mm to 6 mm, this reduction in the radius of curvature resulted in a proportionally increased output current density, reaching a maximum of 9.47×10^{-10} (A cm^{-2}) at the highest strain state. A similar trend was observed under tactile pressure. Stronger finger-pressing forces (Fig. 4d) and smaller hand-bending curvatures (Fig. 4e) produced higher piezoelectric currents, demonstrating a clear strain-to-current transduction relationship. These observations establish that the film exhibits a stable, efficient macroscopic piezoelectric effect suitable for flexible sensing applications. In contrast to macroscopic measurements, PFM and laser Doppler vibrometer (LDV) were employed to probe the piezoelectric response of the PMNTHZO films. Due to the inherent nature of epitaxial thin films, the out-of-plane electromechanical expansion is inevitably influenced by the mechanical constraint of the underlying substrates. Therefore, all nanoscale piezoelectric values reported here represent the effective response ($d_{33,\ eff}$) rather than the absolute intrinsic bulk property. The film deposited on mica exhibited strong out-of-plane piezoresponse, with an effective piezoelectric coefficient $d_{33,\ eff}$ of 98 pm V^{-1} (measured via PFM and calibrated using a standard $BiFeO_3$ (BFO) reference, as detailed in the following section). The exact characterization has been performed on PMNTHZO/Si systems, yielding a $d_{33,\ eff}$ value of 99 pm V^{-1}, delivering a promising performance for MEMS applications. This high $d_{33,\ eff}$ value stems from active nanoscale dipole reorientation, confirming the material's excellent intrinsic piezoelectricity. To validate these nanoscale findings at the macroscopic level, the effective out-of-plane piezoelectric coefficient ($d_{33,\ eff}$) versus DC bias loop curves were directly measured using a LDV. The LDV results (Fig. 5e) reveal that the PMNTHZO film on the rigid STO substrate exhibits a saturated $d_{33,\ eff}$ of approximately 40 ± 5 pm V^{-1}.

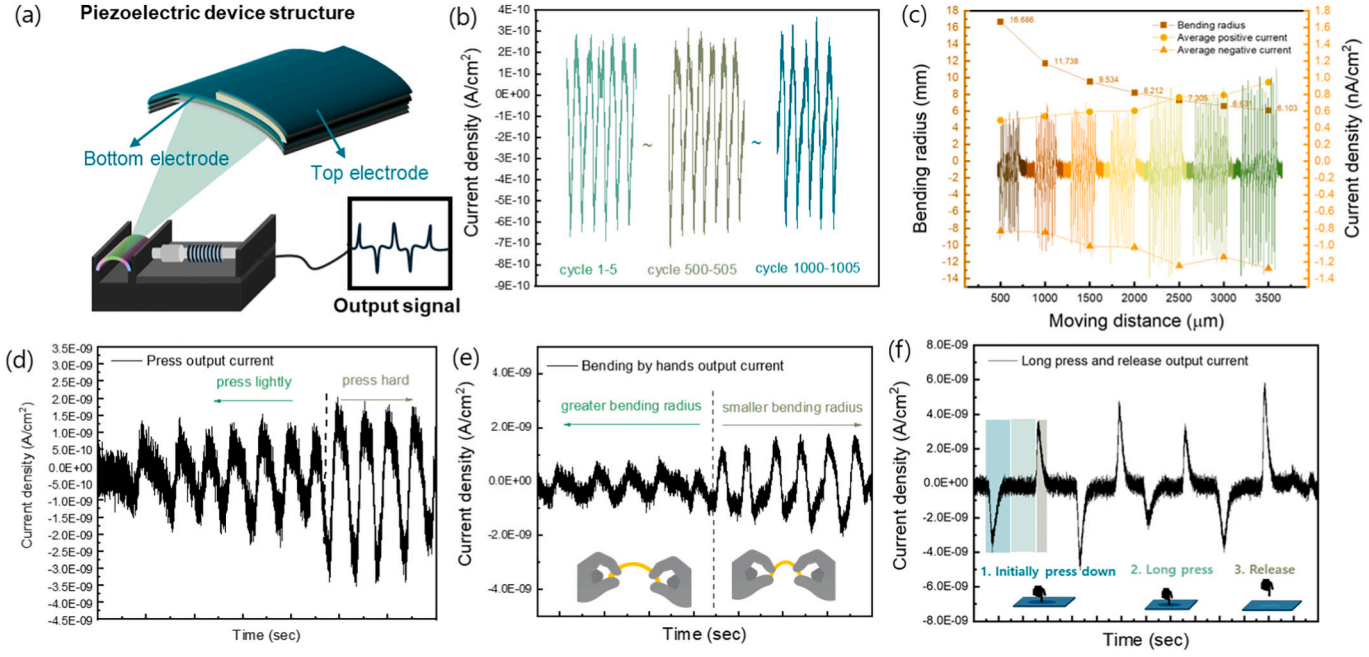

Fig. 4. (a) Schematic of PMNTHZO on mica as a piezoelectric sensor and the experiment method. (b) Bending cycles and stable output current. (c) Output current with varied bending radii. (d) The current signal is produced by finger pressure. (e) The current signal generated by bending the sample manually. (f) The electrical signal output mechanism operates in three stages: an instantaneous negative current pulse is generated immediately upon pressing the sample (Phase 1); the current then returns to an electrically neutral state during sustained pressure (Phase 2); and finally, an instantaneous positive current pulse is generated upon the release of the pressure (Phase 3).

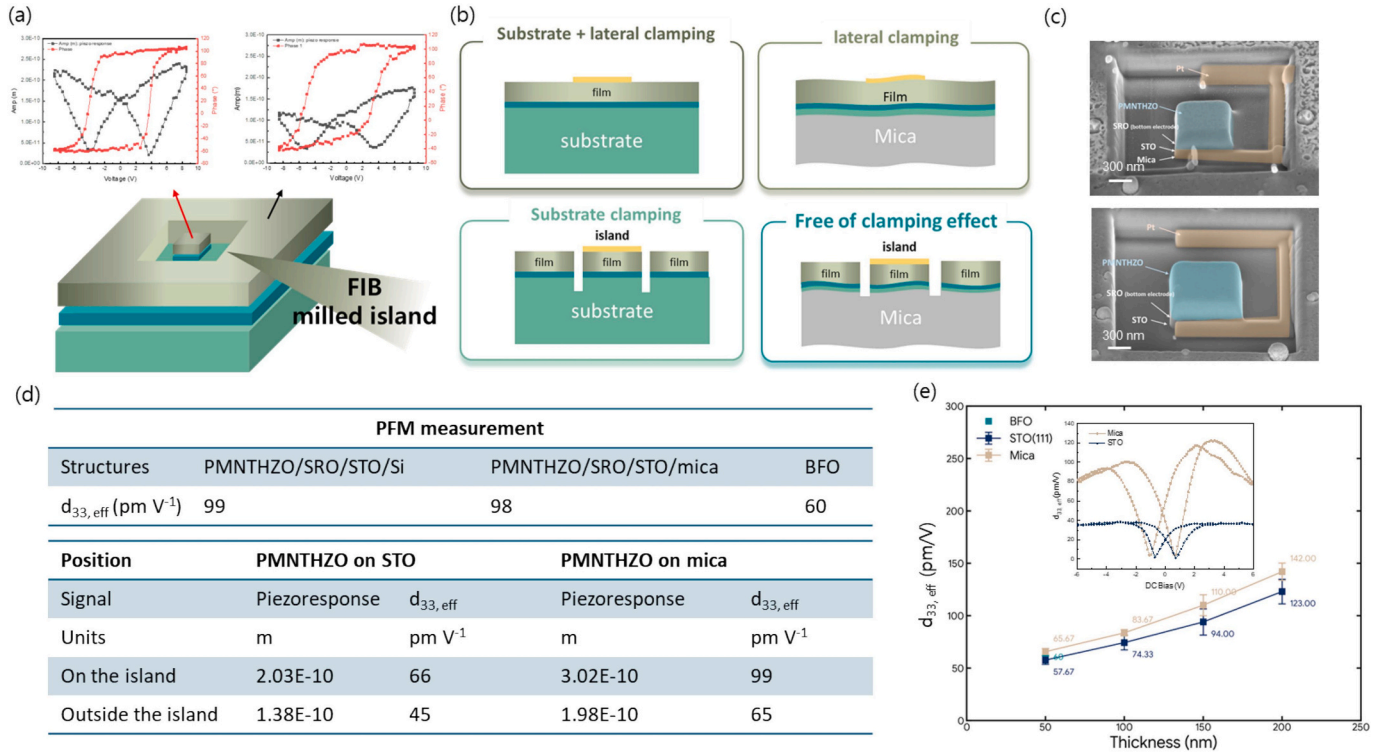

(d)

PFM measurement				
Structures	PMNTHZO/SRO/STO/Si		PMNTHZO/SRO/STO/mica	BFO
$d_{33,\,eff}$ (pm V^{-1})	99		98	60

Position	PMNTHZO on STO		PMNTHZO on mica	
Signal	Piezoresponse	$d_{33,\,eff}$	Piezoresponse	$d_{33,\,eff}$
Units	m	pm V^{-1}	m	pm V^{-1}
On the island	2.03E-10	66	3.02E-10	99
Outside the island	1.38E-10	45	1.98E-10	65

Fig. 5. (a) Explanation of the clamping effect and island structure. Island structures (b) on mica (c) on STO through FIB method. (d) Piezoelectric coefficient of PMNTHZO on STO/Silicon and STO/mica through PFM measurements. (e) Effective d_{33} vs DC bias curve measured from PMNTHZO on STO and mica. Thickness dependent $d_{33,\,eff}$ of PMNTHZO thin film on STO substrate compared with PMNTHZO on mica.

Strikingly, the film grown on the flexible mica substrate (Fig. 5e) demonstrates a significantly enhanced macroscopic piezoresponse, achieving an exceptionally high $d_{33,\,eff\,of}$ 118 ± 6 pm V^{-1} at the saturated polarization state. Further discussion of the influence of high entropy in piezoelectric systems shows that PNRs induce lattice instability and enhance electromechanical coupling, serving as the primary origin of the exceptional piezoelectricity in relaxor ferroelectrics [48]. Guided by this mechanism, our high-entropy design strengthens relaxor behavior by promoting denser and more dynamic PNRs through the high-entropy concept, thereby enabling a "more relaxor-like relaxor" with enhanced piezoelectric performance [47–49,51].

To illustrate the advantage of adopting a mica substrate, we focused on the impact of substrate clamping on the piezoelectric response of thin films. According to the existing literature [67,68] and theoretical calculations [69,70], films grown on rigid substrates suffer from severe clamping effects at extremely thin thicknesses. We used focused ion beam (FIB) milling to define size 1 μm^2 island structures on the continuous PMNTHZO film. The piezoelectric coefficient $d_{33,\,eff}$ of these islands was then measured by PFM and compared to the $d_{33,\,eff}$ of the surrounding continuous film to quantify the release of lateral constraints. In PFM measurements, where the electric field at the probe tip is divergent, the distribution differs significantly from the uniform field generated by parallel electrodes in LDV. Furthermore, issues such as potential decay and an imaging mechanism dominated by the "dielectric gap effect" [71] have been reported. Some studies indicate that microscopic measurements may be lower than macroscopic measurements [72]. Consequently, to mitigate experimental variability, including probe degradation and laser alignment inconsistencies, the PFM measurements were analyzed using a comparative calibration method. Both the target PMNTHZO films and a standard BFO reference sample (with a known d_{33} of ≈ 60 pm V^{-1}) were measured under identical instrumental conditions (e.g., AFM probe, AC driving voltage, and contact force). By extracting the PFM amplitude signals, the $d_{33,\,eff}$ of PMNTHZO was quantitatively determined based on its proportionality to the BFO reference, thereby effectively canceling systematic machine errors. The $d_{33,\,eff}$ values presented below have been converted using the ratio derived from this method (as explained in Fig. S6). Force mapping (Fig. S6) was performed to calculate $d_{33,\,eff}$ using statistical methods. As shown in Fig. 5, measurement of the island revealed a $d_{33,\,eff}$ of 66 pm V^{-1}, a 47.1% increase compared to the continuous film ($d_{33,\,eff}$ ≈ 45 pmV^{-1}), directly confirming the presence of substrate clamping. Moreover, the island on mica shows a $d_{33,\,eff}$ of 99 pm V^{-1}, which is higher than the continuous region of mica (≈ 65 pm V^{-1}). This result reveals that the films on mica are less constrained by the substrate, highlighting a critical feature of 2D-layered muscovite. In parallel, a series of PMNTHZO films with varying thicknesses was grown on the STO and mica substrates (Fig. 5e). As film thickness increases, the structure is expected to approach that of bulk material, leading to a corresponding increase in the piezoelectric response [67,72]. This thickness dependence can be rationalized by stronger substrate clamping in thinner films, which suppresses the effective out-of-plane electromechanical response and reduces extrinsic contributions. Some research reported that the piezoresponse of thin films is constrained by the substrate clamping effect [62,68] (e.g. d_{33} ≈ 130 pm V^{-1} for PZT thin film, but ≈ 600 pm V^{-1} for bulk PZT [68].) As thickness increases, the effective mechanical constraint relaxes, and the measured $d_{33,\,eff}$ recovers. The results strongly support this thickness-dependent release mechanism. By increasing the thickness of the PMNTHZO film regardless of the substrates used, we observed a significant enhancement in the piezoelectric response. For the same thickness, films on mica consistently perform better than those on the STO substrate. This substantial difference confirms that the mica-substrate constraint is reduced relative to the rigid substrate, allowing the intrinsic piezoelectric potential of PMNTHZO to be more fully expressed.

As shown in Fig. S7 and Table S2 [23,73–85], this study demonstrates that the PMNTHZO/mica film achieves a robust piezoelectric coefficient $d_{33,\,eff}$ of up to 124 pm V^{-1}, significantly out- performing flexible polymers (e.g., PVDF-TrFE, ≈ 25.8 pm V^{-1} [81]) and BTO-based

composites (< 50 pm V^{-1} [82,83]). While its $d_{33,\ eff}$ is lower than that of some epitaxial PZT-based films, it maintains high performance with a bending radius of 3.5 mm. The most significant advantage of this work is its exceptional thermal robustness. By maintaining a stable ferroelectric polar state up to 250 °C, it far exceeds the thermal limits of traditional relaxors (e.g., Sm:PMN-PT at 80 °C and PZT/mica at 170 °C). Because macroscopic electromechanical coupling originates directly from these polar nanoregions, this sustained ferroelectric stability provides strong indirect evidence for its piezoelectric reliability at elevated temperatures. This makes PMNTHZO/mica an ideal materials platform with the potential for flexible MEMS and sensors operating in harsh, high-temperature environments where conventional flexible materials typically fail.

4. Conclusions

In summary, this work demonstrates that high-entropy relaxor PMNTHZO thin films effectively combine excellent crystalline quality, thermal robustness, and mechanical flexibility. Through successful epitaxial integration on both silicon and mica, the films exhibit highly coherent structural alignment. The enhanced breakdown strength and sustained ferroelectric stability under extreme thermal stress are strongly attributed to high-entropy engineering, which stabilizes polar nanoregions and suppresses leakage. Furthermore, the mica-based heterostructures exhibit outstanding fatigue resistance under severe bending. By significantly reducing substrate clamping through van der Waals epitaxy, these flexible films achieve an exceptionally high effective piezoelectric response. These findings establish PMNTHZO as a robust material, showing strong potential for future multifunctional flexible sensors and next-generation MEMS technologies.

CRediT authorship contribution statement

Yu-En Pan: Writing – original draft, Investigation, Formal analysis, Data curation, Conceptualization. **Yu-Hao Tu:** Visualization, Investigation. **Li-Hui Tsao:** Visualization, Investigation, Formal analysis, Data curation. **Yu-Ju Lin:** Investigation. **Sheng-Yao Hung:** Investigation, Formal analysis. **Yi-Chun Chen:** Writing – review & editing, Validation, Resources, Data curation. **Mengyao Xiao:** Writing – review & editing, Visualization, Investigation, Formal analysis. **Qibin Zeng:** Writing – review & editing, Validation, Investigation, Formal analysis. **Huajun Liu:** Writing – review & editing, Validation, Resources. **Chengkuo Lee:** Writing – review & editing, Validation, Resources. **Ying-Hao Chu:** Writing – review & editing, Supervision, Resources, Project administration, Funding acquisition, Conceptualization.

Declaration of Generative AI and AI-assisted technologies in the writing process

During the preparation of this work, the authors used Gemini in order to improve the language and grammar, translate technical terms, and assist in visualizing Figure S7 (based on the Table S2 data). After using this tool/service, the authors reviewed and edited the content as needed and take full responsibility for the content of the published article.

Declaration of competing interest

The authors declare the following financial interests/personal relationships which may be considered as potential competing interests: Ying-Hao Chu reports financial support was provided by National Science and Technology Council. If there are other authors, they declare that they have no known competing financial interests or personal relationships that could have appeared to influence the work reported in this paper.

Acknowledgements

The authors acknowledge the funding support by the National Science and Technology Council (NSTC 114-2639-M-007-001-ASP), the National Research Foundation Competitive Research Program (NRF-CRP28-2022-0002), and RIE2025 MTC Individual Research Grant (M22K2c0084).

Appendix A. Supplementary data

Supplementary data to this article can be found online at https://doi.org/10.1016/j.cej.2026.179422.

Data availability

Data will be made available on request.

References

[1] N. Setter, D. Damjanovic, L. Eng, G. Fox, S. Gevorgian, S. Hong, A. Kingon, H. Kohlstedt, N.Y. Park, G.B. Stephenson, I. Stolitchnov, A.K. Taganstev, D. V. Taylor, T. Yamada, S. Streiffer, Ferroelectric thin films: review of materials, properties, and applications, J. Appl. Phys. 100 (5) (2006) 051606, https://doi.org/10.1063/1.2336999.
[2] S. Shetty, J.I. Yang, J. Stitt, S. Trolier-McKinstry, Quantitative and high spatial resolution d_{33} measurement of piezoelectric bulk and thin films, J. Appl. Phys. 118 (17) (2015) 174104, https://doi.org/10.1063/1.4935140.
[3] D. Fu, S. Sogen, H. Suzuki, Intrinsic piezoelectricity of PZT, ACS Appl. Electron. Mater. 6 (9) (2024) 6384–6390, https://doi.org/10.1021/acsaelm.4c00862.
[4] C. Zhong, Q. Jiang, J. Fang, X. Jiang, Thickness and magnetic field dependence of ferroelectric properties in multiferroic $BaTiO_3$–$CoFe_2O_4$ nanocomposite films, J. Appl. Phys. 105 (4) (2009) 044901, https://doi.org/10.1063/1.3078030.
[5] I.-D. Kim, Y. Avrahami, H.L. Tuller, Y.-B. Park, M.J. Dicken, H.A. Atwater, Study of orientation effect on nanoscale polarization in $BaTiO_3$ thin films using piezoresponse force microscopy, Appl. Phys. Lett. 86 (19) (2005) 192907, https://doi.org/10.1063/1.1923173.
[6] Y.F. Hou, W.L. Li, T.D. Zhang, W. Wang, W.P. Cao, X.L. Liu, W.D. Fei, Large piezoelectric response of $BiFeO_3$/$BaTiO_3$ polycrystalline films induced by the low-symmetry phase, Phys. Chem. Chem. Phys. 17 (17) (2015) 11593–11597, https://doi.org/10.1039/C5CP01320H.
[7] N. Ahbab, S. Naz, T.B. Xu, S. Zhang, A comprehensive review of piezoelectric PVDF polymer fabrications and characteristics, Micromachines 16 (2025) 386, https://doi.org/10.3390/mi16040386.
[8] M. Habib, I. Lantgios, K. Hornbostel, A review of ceramic, polymer and composite piezoelectric materials, J. Phys. D. Appl. Phys. 55 (2022) 423002, https://doi.org/10.1088/1361-6463/ac8687.
[9] M.T. Chorsi, E.J. Curry, H.T. Chorsi, R. Das, J. Baroody, P.K. Purohit, H. Ilies, T. D. Nguyen, Piezoelectric biomaterials for sensors and actuators, Adv. Mater. 31 (1) (2019) 1802084, https://doi.org/10.1002/adma.201802084.
[10] M.T. Chorsi, T.T. Le, F. Lin, T. Vinikoor, R. Das, J.F. Stevens, C. Mundrane, J. Park, K.T. Tran, Y. Liu, J. Pfund, Highly piezoelectric, biodegradable, and flexible amino acid nanofibers for medical applications, Sci. Adv. 9 (2023) 6075, https://doi.org/10.1126/sciadv.adg6075.
[11] D. Kim, S.A. Han, J.H. Kim, J.H. Lee, S.W. Kim, S.W. Lee, Biomolecular piezoelectric materials: from amino acids to living tissues, Adv. Mater. 32 (14) (2020) 1906989, https://doi.org/10.1002/adma.201906989.
[12] S. Zhang, F. Li, N.P. Sherlock, J. Luo, H.J. Lee, R. Xia, R.J. Meyer Jr., W. Hackenberger, T.R. Shrout, Recent developments on high curie temperature PIN–PMN–PT ferroelectric crystals, J. Cryst. Growth 318 (2011) 846–850, https://doi.org/10.1016/j.jcrysgro.2010.11.043.
[13] Y. Yamashita, Large electromechanical coupling factors in perovskite binary material system, Jpn. J. Appl. Phys. 33 (1994) 5328, https://doi.org/10.1143/JJAP.33.5328.
[14] M.-H. Tsai, J.-W. Yeh, High-entropy alloys: a critical review, Mater. Res. Lett. 2 (2014) 107–123, https://doi.org/10.1080/21663831.2014.912690.
[15] J.-W. Yeh, S.K. Chen, S.J. Lin, J.Y. Gan, T.S. Chin, T.T. Shun, C.H. Tsau, S.Y. Chang, Nanostructured high-entropy alloys with multiple principal elements: novel alloy design concepts and outcomes, Adv. Eng. Mater. 6 (2004) 299–303, https://doi.org/10.1002/adem.200300567.
[16] W.-L. Hsu, C.-W. Tsai, A.-C. Yeh, J.-W. Yeh, Clarifying the four core effects of high-entropy materials, Nat. Rev. Chem. 8 (2024) 471–485, https://doi.org/10.1038/s41570-024-00602-5.
[17] Y. He, H. Dong, Q. Meng, L. Jiang, W. Shao, L. He, W. Hu, Mica, a potential two-dimensional-crystal gate insulator for organic field-effect transistors, Adv. Mater. 23 (2011) 5502–5507, https://doi.org/10.1002/adma.201103592.
[18] A. Castellanos-Gomez, M. Poot, A. Amor-Amorós, G.A. Steele, H.S.J. van der Zant, N. Agraït, G. Rubio-Bollinger, Mechanical properties of freely suspended atomically thin dielectric layers of mica, Nano Res. 5 (2012) 550–557, https://doi.org/10.1007/s12274-012-0240-3.

[19] J.-Y. Tsai, J.-Y. Chen, C.-W. Huang, H.-Y. Lo, W.-E. Ke, Y.-H. Chu, W.-W. Wu, A high-entropy-oxides-based memristor: outstanding resistive switching performance and mechanisms in atomic structural evolution, Adv. Mater. 35 (2023) 2370298, https://doi.org/10.1002/adma.202370298.

[20] B. Yang, Y. Zhang, H. Pan, W. Si, Q. Zhang, Z. Shen, Y. Yu, S. Lan, F. Meng, Y. Liu, H. Huang, J. He, L. Gu, S. Zhang, L.-Q. Chen, J. Zhu, C.-W. Nan, Y.-H. Lin, High-entropy enhanced capacitive energy storage, Nat. Mater. 21 (2022) 1074–1080, https://doi.org/10.1038/s41563-022-01274-6.

[21] H. Li, Y. Zhou, Z. Liang, H. Ning, X. Fu, Z. Xu, T. Qiu, W. Xu, R. Yao, J. Peng, High-entropy oxides: advanced research on electrical properties, Coatings 11 (2021) 628, https://doi.org/10.3390/coatings11060628.

[22] F. Yang, K.L. Chan, J. Hao, HF-free synthesis of high-entropy MXene-PVA composite film and its flexible nanogenerator, Sci. China-Mater. 68 (2025) 2860–2867, https://doi.org/10.1007/s40843-025-3445-x.

[23] S. Pratihar, A.M. Chandran, A.R. Bhat, P.K.S. Mural, Piezoelectric nanogenerators based on poly (vinylidene fluoride) doped with high entropy oxide nanoparticles for sensitive pressure sensors, ACS Appl. Nano Mater. 7 (2024) 20553–20568, https://doi.org/10.1021/acsanm.4c03569.

[24] Y.-J. Wang, H.C. Lai, Y.A. Chen, R. Huang, T. Hsin, H.J. Liu, R. Zhu, P. Gao, C. Li, P. Yu, Y.C. Chen, J. Li, Y.C. Chen, J.W. Yeh, Y.H. Chu, High entropy nonlinear dielectrics with superior thermally stable performance, Adv. Mater. 35 (2023) 2304128, https://doi.org/10.1002/adma.202304128.

[25] G.T. Kovacs, Micromachined Transducers Sourcebook vol. 2, WCB/McGraw-Hill, New York, 1998.

[26] M.J. Madou, Fundamentals of Microfabrication: the Science of Miniaturization, CRC Press, 2018, https://doi.org/10.1201/9781482274004.

[27] H. Qu, CMOS MEMS fabrication technologies and devices, Micromachines 7 (2016) 14, https://doi.org/10.3390/mi7010014.

[28] Y.-H. Chu, Van der Waals oxide heteroepitaxy, NPJ Quantum Mater. 2 (2017) 67, https://doi.org/10.1038/s41535-017-0069-9.

[29] J. Jiang, Y. Bitla, C.-W. Huang, T.H. Do, H.-J. Liu, Y.-H. Hsieh, C.-H. Ma, C.-Y. Jang, Y.-H. Lai, P.-W. Chiu, W.-W. Wu, Y.-C. Chen, Y.-C. Chen, Y.-H. Chu, Flexible ferroelectric element based on van der Waals heteroepitaxy, Sci. Adv. 3 (2017) e1700121, https://doi.org/10.3791/57221-v.

[30] L. Zhen, M. Cui, X. Bai, J. Jiang, X. Ma, M. Wang, J. Liu, B. Yang, Thin, flexible hybrid-structured piezo- electric sensor array with enhanced resolution and sensitivity, Nano Energy 131 (2024) 110188, https://doi.org/10.1016/j.nanoen.2024.110188.

[31] J. Liu, H. Tan, X. Zhou, W. Ma, C. Wang, N.M. Tran, W. Lu, F. Chen, J. Wang, H. Zhang, Piezoelectric thin films and their applications in MEMS: a review, J. Appl. Phys. 137 (2) (2025), https://doi.org/10.1063/5.0244749.

[32] Z. Lu, G. Wang, L. Li, Y. Huang, A. Feteira, W. Bao, A.K. Kleppe, F. Xu, D. Wang, I. M. Reaney, In situ poling X-ray diffraction studies of lead-free $BiFeO_3$–$SrTiO_3$ ceramics, Mater. Today Phys. 19 (2021) 100426, https://doi.org/10.1016/j.mtphys.2021.100426.

[33] S. Taleb, M. Badillo, F.J. Flores-Ruiz, M. Acuautla, From synthesis to application: high-quality flexible piezo- electric sensors fabricated from tetragonal $BaTiO_3$/P (VDF-TrFE) composites, Sens. Actuators A Phys. 361 (2023) 114585, https://doi.org/10.1016/j.sna.2023.114585.

[34] Y. Tanaka, S. Okamoto, K. Hashimoto, R. Takayama, T. Harigai, H. Adachi, E. Fujii, High electromechanical strain and enhanced temperature characteristics in lead-free (Na, Bi)TiO_3-$BaTiO_3$ thin films on Si substrates, Sci. Rep. 8 (2018) 7847, https://doi.org/10.1038/s41598-018-26309-4.

[35] F. Qi, L. Xu, Y. He, H. Yan, H. Liu, PVDF-based flexible piezoelectric tactile sensors: review, Cryst. Res. Technol. 58 (2023) 2300119, https://doi.org/10.1002/crat.202300119.

[36] W. Fan, R. Lei, H. Dou, Z. Wu, L. Lu, S. Wang, X. Liu, W. Chen, M. Rezakazemi, T. M. Aminabhavi, Y. Li, Sweat permeable and ultrahigh strength 3D PVDF piezoelectric nanoyarn fabric strain sensor, Nat. Commun. 15 (1) (2024) 3509, https://doi.org/10.1038/s41467-024-47810-7.

[37] P.-H. Ducrot, I. Dufour, C. Ayela, Optimization of PVDF-TrFE processing conditions for the fabrication of organic MEMS resonators, Sci. Rep. 6 (1) (2016) 19426, https://doi.org/10.1038/srep19426.

[38] J. Han, M. Saravanapavanantham, M.R. Chua, J.H. Lang, V. Bulović, A versatile acoustically active surface based on piezoelectric microstructures, Microsyst. Nanoeng. 8 (1) (2022) 55, https://doi.org/10.1038/s41378- 022-00384-0.

[39] M. Xu, Y. Wen, D. Li, C. Xiong, Q. Yang, J. Xu, Z. Shi, Piezoelectric poly-L-lactic acid for next-generation energy harvesting and biomedical applications, Chem. Eng. J. 512 (2025) 162536, https://doi.org/10.1016/j.cej.2025.162536.

[40] M. Xiao, A. Xu, Z. Sui, W. Zhang, H. Liu, C. Lee, Multifunctional MEMS, NEMS, micro/nano-structures enabled by piezoelectric and ferroelectric effects, Nanoscale Horiz. 10 (11) (2025) 2744–2771, https://doi.org/10.1039/D5NH00386E.

[41] R.M. Pinto, V. Gund, R.A. Dias, K.K. Nagaraja, K.B. Vinayakumar, CMOS-integrated aluminum nitride MEMS: a review, J. Microelectromech. Syst. 31 (4) (2022) 500–523, https://doi.org/10.1109/JMEMS.2022.3172766.

[42] S.-H. Baek, C.-B. Eom, Epitaxial integration of perovskite-based multifunctional oxides on silicon, Acta Mater. 61 (2013) 2734–2750, https://doi.org/10.1016/j.actamat.2012.09.073.

[43] R.A. McKee, F.J. Walker, M.F. Chisholm, Crystalline oxides on silicon: the first five monolayers, Phys. Rev. Lett. 81 (1998) 3014, https://doi.org/10.1103/PhysRevLett.81.3014.

[44] L. Lu, Atomic scale understanding of the epitaxy of perovskite oxides on flexible mica substrate, Adv. Mater. Interfaces 7 (2020) 1901265, https://doi.org/10.1002/admi.201901265.

[45] R. Liang, S. Ke, The competition between van der Waals and ionic interactions at the $SrTiO_3$/mica heterointerface, Appl. Phys. Lett. 126 (2025) 111601, https://doi.org/10.1063/5.0260844.

[46] Y. Du, B. Xu, G. Wang, Y. Miao, B. Li, Z. Kong, Y. Dong, W. Wang, H.H. Radamson, Review of highly mismatched III-V heteroepitaxy growth on (001) silicon, Nanomaterials 12 (5) (2022) 741, https://doi.org/10.3390/nano12050741.

[47] F. Li, S. Zhang, Z. Xu, L.-Q. Chen, The contributions of polar nanoregions to the dielectric and piezoelectric responses in domain-engineered relaxor-$PbTiO_3$ crystals, Adv. Funct. Mater. 27 (18) (2017) 1700310, https://doi.org/10.1002/adfm.201700310.

[48] G. Xu, J. Wen, C. Stock, P.M. Gehring, Phase instability induced by polar nanoregions in a relaxor ferroelectric system, Nat. Mater. 7 (7) (2008) 562–566, https://doi.org/10.1038/nmat2196.

[49] X. Shi, J. Wang, J. Xu, X. Cheng, H. Huang, Quantitative investigation of polar nanoregion size effects in relaxor ferroelectrics, Acta Mater. 237 (2022) 118147, https://doi.org/10.1016/j.actamat.2022.118147.

[50] H. Fu, R.E. Cohen, Polarization rotation mechanism for ultrahigh electromechanical response in single-crystal piezoelectrics, Nature 403 (6767) (2000) 281–283, https://doi.org/10.1038/35002022.

[51] Y. Gao, W. Qiao, X. Lou, Z. Song, X. Zhu, L. He, B. Yang, Y. Hu, J. Shao, D. Wang, Z. Chen, S. Zhang, Ultrahigh energy storage in tungsten bronze dielectric ceramics through a weakly coupled relaxor design, Adv. Mater. 36 (11) (2024) 2310559, https://doi.org/10.1002/adma.202310559.

[52] M. Wang, Y. Lin, B. Zheng, Q. Yuan, H. Yang, Optimized energy storage performances via high- entropy design in KNN-based relaxor ferroelectric ceramics, Chem. Eng. J. 499 (2024) 156447, https://doi.org/10.1016/j.cej.2024.156447.

[53] L. Pintilie, I. Vrejoiu, D. Hesse, G. LeRhun, M. Alexe, Ferroelectric polarization-leakage current relation in high quality epitaxial Pb(Zr, Ti)O_3 films, Phys. Rev. B 75 (10) (2007) 104103, https://doi.org/10.1103/PhysRevB.75.104103.

[54] H. Peng, T. Wu, Z. Liu, Z. Fu, D. Wang, Y. Hao, F. Xu, G. Wang, J. Chu, High entropy relaxor ferroelectric ceramics for ultrahigh energy storage, Nat. Commun. 15 (1) (2024) 5232, https://doi.org/10.1038/s41467-024-50284-2.

[55] G. Deng, G. Li, A. Ding, Q. Yin, Evidence for oxygen vacancy inducing spontaneous normal-relaxor transition in complex perovskite ferroelectrics, Appl. Phys. Lett. 87 (2005) 192905, https://doi.org/10.1063/1.2125110.

[56] I. Stolichnov, A. Tagantsev, Space-charge influenced-injection model for conduction in Pb (Zr_x Ti_{1-x}) O_3 thin films, J. Appl. Phys. 84 (1998) 3216–3225, https://doi.org/10.1063/1.369518.

[57] B. Akkopru-Akgun, et al., Leakage current characteristics and DC resistance degradation mechanisms in Nb doped PZT films, J. Appl. Phys. 129 (2021) 174102, https://doi.org/10.1063/5.0041927.

[58] P.F. Baude, C. Ye, D.L. Polla, Deep level transient spectroscopy characterization of ferroelectric Pb (Zr, Ti) O_3 thin films, Appl. Phys. Lett. 64 (1994) 2670–2672, https://doi.org/10.1063/1.111487.

[59] T. Tsurumi, K. Soejima, T.K.T. Kamiya, M.D.M. Daimon, Mechanism of diffuse phase transition in relaxor ferroelectrics, Jpn. J. Appl. Phys. 33 (4R) (1994) 1959, https://doi.org/10.1143/JJAP.33.195.

[60] M. Lallart, Ferroelectrics: characterization and modeling, BoD-Books on Demand, 2011, https://doi.org/10.5772/946.

[61] L.K. Pradhan, M. Kar, Concept to Applications, in: Multifunctional ferroelectric materials, 2021, p. 49, https://doi.org/10.5772/intechopen.96185.

[62] V. Nagarajan, A. Roytburd, A. Stanishevsky, S. Prasertchoung, T. Zhao, L.Q. Chen, J. Melngailis, O. Au- ciello, R. Ramesh, Dynamics of ferroelastic domains in ferroelectric thin films, Nat. Mater. 2 (1) (2003) 43–47, https://doi.org/10.1038/nmat800.

[63] M.-F. Tsai, Y.-Z. Zheng, S.-C. Lu, J.-D. Zheng, H. Pan, C.-G. Duan, P. Yu, R. Huang, Y.-H. Chu, Antiferroelec- tric anisotropy of epitaxial $PbHfO_3$ films for flexible energy storage, Adv. Funct. Mater. 31 (42) (2021) 2105060, https://doi.org/10.1002/adfm.202105060.

[64] X. Liu, C. Wei, T. Sun, F. Zhang, H. Li, L. Liu, Y. Peng, H. Li, M. Hong, A $BaTiO_3$-based flexible ferroelectric capacitor for non-volatile memories, J. Mater. 11 (2) (2025) 100870, https://doi.org/10.1016/j.jmat.2024.04.001.

[65] X. Liu, Y. Peng, F. Zhang, T. Sun, Y. Peng, L. Wen, H. Li, Enhanced performance of flexible $BiFeO_3$ ferroelectric memory with Mica substrate via $SrTiO_3$ buffer layer, Sci. Rep. 14 (1) (2024) 25292, https://doi.org/10.1038/s41598-024-77119-w.

[66] H. Qi, X. Xia, C. Zhou, P. Xiao, Y. Wang, Y. Deng, Ferroelectric properties of the flexible Pb ($Zr_{0.52}$ $Ti_{0.48}$) O_3 thin film on mica, J. Mater. Sci. Mater. Electron. 31 (4) (2020) 3042–3047, https://doi.org/10.1007/s10854-019-02848-y.

[67] R.N. Torah, S.P. Beeby, N.M. White, Experimental investigation into the effect of substrate clamping on the piezoelectric behavior of thick-film PZT elements, J. Phys. D. Appl. Phys. 37 (7) (2004) 1074–1078, https://doi.org/10.1088/0022-3727/37/7/019.

[68] D.M. Kim, C.-B. Eom, V. Nagarajan, J. Ouyang, R. Ramesh, V. Vaithyanathan, D. G. Schlom, Thickness dependence of structural and piezoelectric properties of epitaxial Pb ($Zr_{0.52}Ti_{0.48}$) O_3 films on Si and $SrTiO_3$ substrates, Appl. Phys. Lett. 88 (14) (2006), https://doi.org/10.1063/1.2185614.

[69] A. Arnau, D. Soares, Piezoelectric Transducers and Applications 2004, Springer, 2004, https://doi.org/10.1007/978-3-540-77508-9.

[70] S. Priya, J. Ryu, C.-S. Park, J. Oliver, J.-J. Choi, D.-S. Park, Piezoelectric and magnetoelectric thick films for fabricating power sources in wireless sensor nodes, Sensors 9 (8) (2009) 6362–6384, https://doi.org/10.3390/s90806362.

[71] S. Eom, P. Kavle, D. Kang, Y. Kim, L.W. Martin, S. Hong, Unveiling the nanoscale dielectric gap and its influence on ferroelectric polarization switching in scanning probe microscopy, Adv. Funct. Mater. 35 (11) (2025) 2406944, https://doi.org/10.1002/adfm.202406944.

[72] A. Gruverman, M. Alexe, D. Meier, Piezoresponse force microscopy and nanoferroic phenomena, Nat. Commun. 10 (1) (2019) 1661, https://doi.org/10.1038/s41467-019-09650-8.
[73] R. Zhang, Y. Ding, N. Liu, W. Tang, Y. Wang, Y. Yang, Y. Wang, G. Yuan, High macroscopic piezoelectric d_{33} of the nm-thick flexible PZT ferroelectric film, J. Mater. Sci. Mater. Electron. 35 (4) (2024) 298, https://doi.org/10.1007/s10854-024-12040-6.
[74] C. Li, J. Si, X. Yuan, W. Wang, G. Wang, X. Lin, S. Huang, C. Yang, Flexible all-inorganic $BiFeO_3$-based film with high piezoelectric coefficient for energy harvesting and sensing, J. Mater. Sci. Mater. Electron. 35 (26) (2024) 1745, https://doi.org/10.1007/s10854-024-13514-3.
[75] P. Lv, J. Qian, C. Yang, T. Liu, Y. Wang, D. Wang, S. Huang, X. Cheng, Z. Cheng, Flexible all-inorganic Sm-doped PMN-PT film with ultrahigh piezoelectric coefficient for mechanical energy harvesting, motion sensing, and human-machine interaction, Nano Energy 97 (2022) 107182, https://doi.org/10.1016/j.nanoen.2022.107182.
[76] X. Zhang, Y. Wang, X. Gao, Y. Ji, F. Qian, J. Fan, H. Wang, L. Qiu, W. Li, H. Yang, High-temperature and flexible piezoelectric sensors for lamb-wave-based structural health monitoring, ACS Appl. Mater. Interfaces 13 (40) (2021) 47764–47772, https://doi.org/10.1021/acsami.1c13704.
[77] W. Gao, L. You, Y. Wang, G. Yuan, Y.-H. Chu, Z. Liu, J.-M. Liu, Flexible PbZr0.52Ti0.48O3 capacitors with giant piezoelectric response and dielectric tunability, Adv. Electron. Mater. 3 (8) (2017) 1600542, https://doi.org/10.1002/aelm.201600542.
[78] D. Wang, G. Yuan, G. Hao, Y. Wang, All-inorganic flexible piezoelectric energy harvester enabled by two- dimensional mica, Nano Energy 43 (2018) 351–358, https://doi.org/10.1016/j.nano.
[79] S. Liu, D. Zou, X. Yu, Z. Wang, Z. Yang, Transfer-free PZT thin films for flexible nanogenerators derived from a single-step modified sol-gel process on 2D mica, ACS Appl. Mater. Interfaces 12 (49) (2020) 54991–54999, https://doi.org/10.1021/acsami.0c16973.
[80] S. Liu, Z. Zhang, Y. Shan, Y. Hong, F. Farooqui, F.S. Lam, W.-H. Liao, Z. Wang, Z. Yang, A flexible and lead-free BCZT thin film nanogenerator for biocompatible energy harvesting, Mater. Chem. Front. 5 (12) (2021) 4682–4689, https://doi.org/10.1039/D1QM00145K.
[81] S. Hajra, V. Vivekananthan, M. Sahu, G. Khandelwal, N.P.M.J. Raj, S.-J. Kim, Triboelectric nanogenerator using multiferroic materials: an approach for energy harvesting and self-powered magnetic field detection, Nano Energy 85 (2021) 105964, https://doi.org/10.1016/j.nanoen.2021.105964.
[82] X. Li, Y. Wang, T. He, Q. Hu, Y. Yang, Preparation of PVDF flexible piezoelectric film with high β-phase content by matching solvent dipole moment and crystallization temperature, J. Mater. Sci. Mater. Electron. 30 (22) (2019) 20174–20180, https://doi.org/10.1007/s10854-019-02400-y.
[83] A. Renteria, V.H. Balcorta, C. Marquez, A.A.A. Rodriguez, I. Renteria-Marquez, J. Regis, B. Wilburn, S. Patterson, D. Espalin, T.-L. Tseng, et al., Direct ink writes multi-material printing of PDMS-BTO composites with MWCNT electrodes for flexible force sensors, Flex. Print. Electron. 7 (1) (2022) 015001, https://doi.org/10.1088/2058-8585/ac442e.
[84] M. Maturi, L. Migliorini, S.M. Villa, T. Santaniello, N. Fernandez-Delgado, S. I. Molina, P. Milani, A.S. de León, M.C. Franchini, 3D-printing of highly piezoelectric barium titanate polymer nanocomposites with surface-modified nanoparticles at low loadings, Adv. Funct. Mater. 35 (1) (2025) 2407077, https://doi.org/10.1002/adfm.202407077.
[85] F. Zhan, F. Yao, W. Gong, Z. Wang, C. Wang, J. Wan, Highly flexible KNN-PA11 Piezoceramics composite films for efficient energy harvesting, J. Alloys Compd. (2025) 184719, https://doi.org/10.1016/j.jallcom.2025.184719.